

Article

# Kerf Geometry and Surface Roughness Optimization in CO<sub>2</sub> Laser Processing of FFF Plates Utilizing Neural Networks and Genetic Algorithms Approaches

John D. Kechagias <sup>1,\*</sup>, Nikolaos A. Fountas <sup>2</sup>, Konstantinos Ninikas <sup>1</sup> and Nikolaos M. Vaxevanidis <sup>2,\*</sup>

<sup>1</sup> Design & Manufacturing Lab (DML), Department of FWSD, University of Thessaly, 43100 Karditsa, Greece

<sup>2</sup> Department of Mechanical Engineering, School of Pedagogical and Technological Education (ASPETE), 15122 Amarousion, Greece

\* Correspondence: jkechag@uth.gr (J.D.K.); vaxev@aspete.gr (N.M.V.)

**Abstract:** This work deals with the experimental investigation and multi-objective optimization of mean kerf angle (A) and mean surface roughness (Ra) in laser cutting (LC) fused filament fabrication (FFF) 3D-printed (3DP), 4 mm-thick polylactic acid (PLA) plates by considering laser feed (F) and power (P) as the independent control parameters. A CO<sub>2</sub> laser apparatus was employed to conduct machining experiments on 27 rectangular workpieces. An experimental design approach was adopted to establish the runs according to full-combinatorial design with three repetitions, resulting in 27 independent experiments. A customized response surface experiment was formulated to proceed with regression equations to predict the responses and examine the solution domain continuously. After examining the impact of F and P on mean A and mean Ra, two reliable prediction models were generated to model the process. Furthermore, since LC is a highly intricate, non-conventional machining process and its control variables affect the responses in a nonlinear manner, A and Ra were also predicted using an artificial neural network (NN), while its resulting performance was compared to the predictive regression models. Finally, the regression models served as objective functions for optimizing the responses with an intelligent algorithm adopted from the literature.

**Keywords:** laser; processing; FFF; 3D printing; surface roughness; kerf angle; multi-objective optimization; neural networks; grey wolf algorithm



**Citation:** Kechagias, J.D.; Fountas, N.A.; Ninikas, K.; Vaxevanidis, N.M. Kerf Geometry and Surface Roughness Optimization in CO<sub>2</sub> Laser Processing of FFF Plates Utilizing Neural Networks and Genetic Algorithms Approaches. *J. Manuf. Mater. Process.* **2023**, *7*, 77. <https://doi.org/10.3390/jmmp7020077>

Academic Editors: Antonio Riveiro and Rafael Comesaña

Received: 20 February 2023

Revised: 14 April 2023

Accepted: 17 April 2023

Published: 18 April 2023



**Copyright:** © 2023 by the authors. Licensee MDPI, Basel, Switzerland. This article is an open access article distributed under the terms and conditions of the Creative Commons Attribution (CC BY) license (<https://creativecommons.org/licenses/by/4.0/>).

## 1. Introduction

Laser cutting (LC) is a thermal processing technique that severs the material by locally melting it, using a repeatedly pulsing or continuously immersed laser beam. As a result, a kerf is formed through relative motion between the beam and the workpiece surface. Laser cutting is used to cut an extensive range of materials (composites, papers, wooden plates, ceramics, metals, inorganics, organics, etc.) without regard for their hardness or electrical conductivity [1–3]. Laser beam cutting and other laser processing methods (laser finishing, engraving, welding, etc.) are applied extensively in many industrial applications, particularly in automotive and aerospace industries [4–6]. The post-processing of the objects formed by conventional or non-conventional techniques is critical for enhancing the final product grade [7–9]. As a result, fused filament fabrication (FFF) or material extrusion (MEX) is growing extensively in numerous engineering and industrial fields [10–12]. A workpiece is created by adding layers of material [13–15]. In addition, the filament material extrusion process creates opportunities for enhancing sustainability issues due to the customized demand for energy and materials [16–18]. One of the most naturally used biopolymers is polylactic acid (PLA), with the second largest volume of applications worldwide [19]. It is a recyclable, biodegradable, and bioactive thermoplastic originating from renewable sources such as sugarcane or corn starch. Moreover, PLA is a promising

polymer for several customized applications, having the most negligible environmental impact compared to other thermopolymers [20,21].

Numerous investigations have studied various laser beam processing techniques. For example, different thermoplastics such as polypropylene (PP), polyethylene (PE), and phosphorylcholine (PC) thin plates were cut with a range of laser variable parameters, revealing that with low laser feed, the result has a more positive outcome when using a high-power laser [22,23]. In addition, several researchers have studied polymethyl methacrylate (PMMA) thin plates on different laser beam settings by investigating the kerf angle, surface roughness, and heat-affected zone [24–26].

Zhou and Mahdavian studied the cutting of nonmetallic materials experimentally and theoretically using a CO<sub>2</sub> laser [27]. In addition, the cutting performance of the laser beam onto thin plates of PLA, ABS, PET-G, PLA/Wood, and PLA/CB manufactured by the material extrusion process has been studied for dimensional and surface property improvement [28–33].

Combinatorial experimental methodology contributes to well-organized documentation correlating a process's input parameters to its corresponding outputs [34], as does response surface methodology [35,36]. The DOE approach is prominent in the full and fractional factorial design (FD) [37]. In order to attain the optimum results during a cut, efforts to concurrently optimize two or more control factors have been carried out, depending vastly on the test workpiece [38–41]. The post-processing of FFF is vital for most products, especially when strict precision requirements are imposed [42]. Note here that the shape accuracy of the FFF parts is affected by the 3D printing processing parameters such as layer thickness, nozzle temperature, printing speed, etc., and their inappropriate tuning causes material overflow, overheating, and gaps between layers, which in turn results in uneven corners and curling surfaces [17]. Therefore, precision laser-assisted post-processing can be an alternative to conventional machining for precision customized FFF parts used in assemblies or mechanisms.

The present study optimizes the surface properties of a PLA 3D-printed (3DP) thin plate processed by a laser beam utilizing soft computing techniques. The surface properties specified were the geometry of the mean kerf angle ( $A$ ) and the cut's mean surface roughness ( $R_a$ ), as these two are the most critical according to the literature. It is worth mentioning that the published work on optimizing the laser cutting of 3D-printed parts is somewhat limited. The authors designed this work to have two key processing parameters after the literature review, and the research aim was mainly the multi-parameter, multi-objective optimization of CO<sub>2</sub> laser cutting of a 3D-printed material (PLA thin plates) for the case of two inputs and two outputs with experimental design, mathematical RSM (regression surface models) and NN modeling, and MOGWO (grey wolf optimization algorithm) metaheuristic optimization algorithm adopted from the literature.

Therefore, additional research and experimentation are needed to determine the probability of successfully executing laser processing on 3DP thin workpieces on an industrial basis. This work displays how laser beam feed ( $F$ ) and power ( $P$ ) impact the kerf angle ( $A$ ) and mean surface roughness ( $R_a$ ) of a 3DP thermoplastic (PLA) during LC. Likewise, the laser feed and power results have been examined through response surface analysis and residual analysis. Cutting experiments were conducted using the full combinatorial approach, with three repetitions following the design of experiments (DOE) methodology. In contrast, regression analysis and artificial neural networks (ANN) were implemented to model the process. Finally, a multi-objective optimization problem was formulated and solved by implementing a modern metaheuristic algorithm found in the broader literature.

## 2. Materials and Methods

Test samples were manufactured with the filament material extrusion (FME) technique (Ender 3, Creality, Shenzhen, China) with a 0.4 mm nozzle diameter. Initially, twenty-seven  $25 \times 25 \times 4$  (mm) PLA cuboid thin plates were FME manufactured. Then, they were cut into  $15 \times 15$  (mm) rectangular samples (see Figure 1b,c). The PLA 3DP cuboid parts

were manufactured adopting the 0.2 mm layer height, 100% infill, 100% flow rate, zero raster angle, 220 °C nozzle temperature, 55 °C bed temperature, 2 shells (perimeters, floors, roofs), 100% fan, and 45 mm/s deposition speed. Note that the laser beam was positioned vertically or parallel to deposited strands of the FME plates during all laser cut work presented in this study.

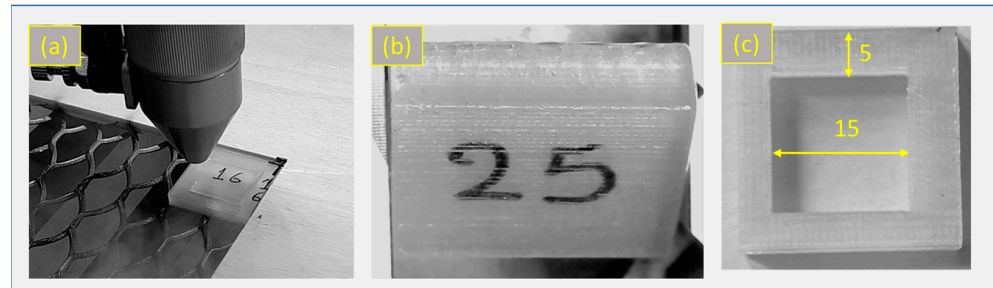


**Figure 1.** (a) Laser cutting work, (b) final cuboid part (15 × 15 mm No 25), and (c) remaining ring after cutting.

The laser cut of samples was realized by a budget (BCL 1325B; 150 W max, 10.6 μm wavelength; 2 mm nozzle diameter; convergent type; 1 bar pressure air) continuous CO<sub>2</sub> laser. The focus lens adjustments (three reflection mirrors and a focus lens) and all the laser details were presented in [3]. Therefore, a 0.3 mm laser spot was achieved at an 8 mm stand-off distance. Then, the samples were placed on the laser working table, as presented in Figure 1a.

The samples were cut with 8, 13, and 18 mm/s feed and 82.5, 90, and 97.5 W power (Table 1). The parameter level selection follows the previous work’s cutting setting of PMMA plates [3]. Note that the specific gravity of PMMA and PLA is very close (about 1.2 g/cm<sup>3</sup>), so all combinations were considered suitable for cutting the PLA samples. The nine combinations of the different sets of laser feed and power were repeated three times, resulting in twenty-seven independent experiments (Table 2). All experiments were cut in the laser bed at the same position and orientation (Figure 1a). Mean results from the measurements of kerf angles and roughness corresponding to cut surfaces along the X and Y axes were finally kept as final outputs for further statistical analysis.

**Table 1.** LC parameters.

Laser Parameters	Symbol	Levels		
Feed	F (mm/s)	1	2	3
Power	P (W)	8	13	18
		82.5	90.0	97.5

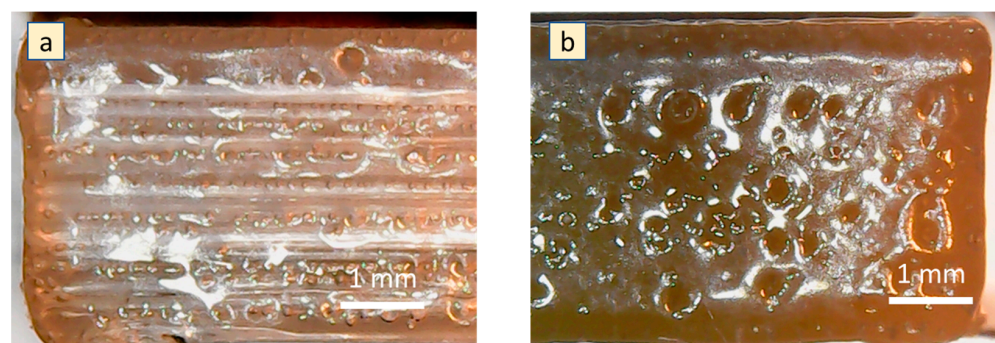
**Table 2.** Laser cutting experiments and corresponding results for A and Ra responses.

a/a	F (mm/s)	P (W)	Mean A (°)	Mean Ra (μm)
1	8	82.5	1.596	1.72
2	8	82.5	1.438	1.74
3	8	82.5	1.519	1.88
4	8	90.0	1.465	1.51
5	8	90.0	1.612	1.50
6	8	90.0	1.537	1.42
7	8	97.5	1.216	0.81
8	8	97.5	1.307	0.88
9	8	97.5	1.259	1.06
10	13	82.5	1.108	1.16
11	13	82.5	1.054	1.04
12	13	82.5	1.094	1.05

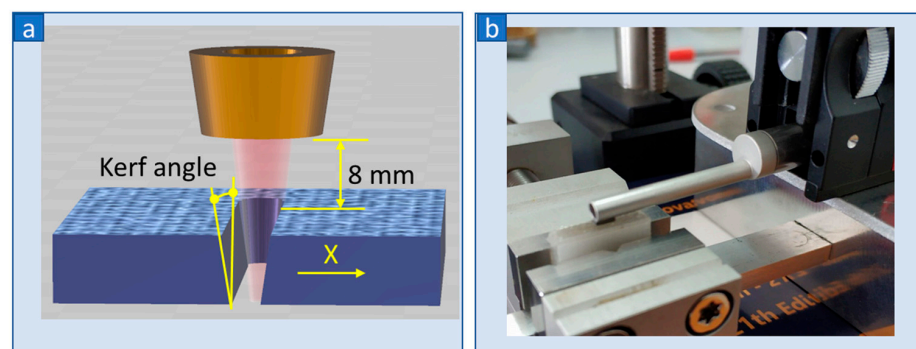
**Table 2.** *Cont.*

a/a	F (mm/s)	P (W)	Mean A (°)	Mean Ra (μm)
13	13	90.0	1.076	0.92
14	13	90.0	1.012	1.00
15	13	90.0	1.094	1.07
16	13	97.5	1.088	1.09
17	13	97.5	1.079	2.08
18	13	97.5	1.102	1.46
19	18	82.5	0.965	4.42
20	18	82.5	1.012	2.23
21	18	82.5	0.894	2.53
22	18	90.0	0.989	2.61
23	18	90.0	0.945	2.42
24	18	90.0	0.917	2.37
25	18	97.5	1.009	6.15
26	18	97.5	0.897	6.19
27	18	97.5	0.884	5.92

The geometric measurements were taken utilizing the ImageJ software. Photos were taken utilizing a budget microscope and the Cooling Tech Microscope software. Figure 2a presents a cut parallel to strands, whereas Figure 2b presents a cut perpendicular to strands. Surface roughness measurements were taken with the DIAVITE profilometer (4 mm sample length, 0.001 μm accuracy). The Ra measurements were taken in the middle of the cutting surface on both X and Y sides and about 2 mm from the top surface.

**Figure 2.** (a) Parallel cutting, (b) perpendicular cutting.

The cutting surface and the vertical plane formed the kerf angle (see Figure 3a). The same microscope mentioned above examined kerf angles for each test sample. Ra was measured by preparing a special fixture device for clamping the test specimens, as depicted in Figure 3b.

**Figure 3.** (a) Kerf angle, (b) specimen, and Ra measurements.

### 3. Results and Discussion

#### 3.1. Full Quadratic Regression Models for CO<sub>2</sub> Laser Cutting Objectives

Based on the results obtained for the two objectives of kerf angle and surface roughness, two second-order regression models were generated for correlating laser feed and laser power to kerf angle and surface roughness. The general regression equation for producing the models is given in Equation (1):

$$y = \beta_0 + \sum_{i=1}^k \beta_i x_i + \sum_{i=1}^k \beta_{ij} x_i^2 + \sum_i \sum_j \beta_{ij} x_i x_j \tag{1}$$

$y$  is the response—mean kerf angle  $A$  (°) and surface roughness ( $R_a$ ,  $\mu\text{m}$ ), “ $\beta$ ” are the regression coefficients as computed by the least square fit, and  $x_i$  is the different independent factors for  $i = 1$  to  $k$ , where  $k$  is the total number of independent (control) factors (parameters). Nonlinearity and effects referring to laser feed and laser power on mean  $A$  and mean  $R_a$  have been examined with the aid of surface and contour plots utilizing the Minitab17 (Figure 4).

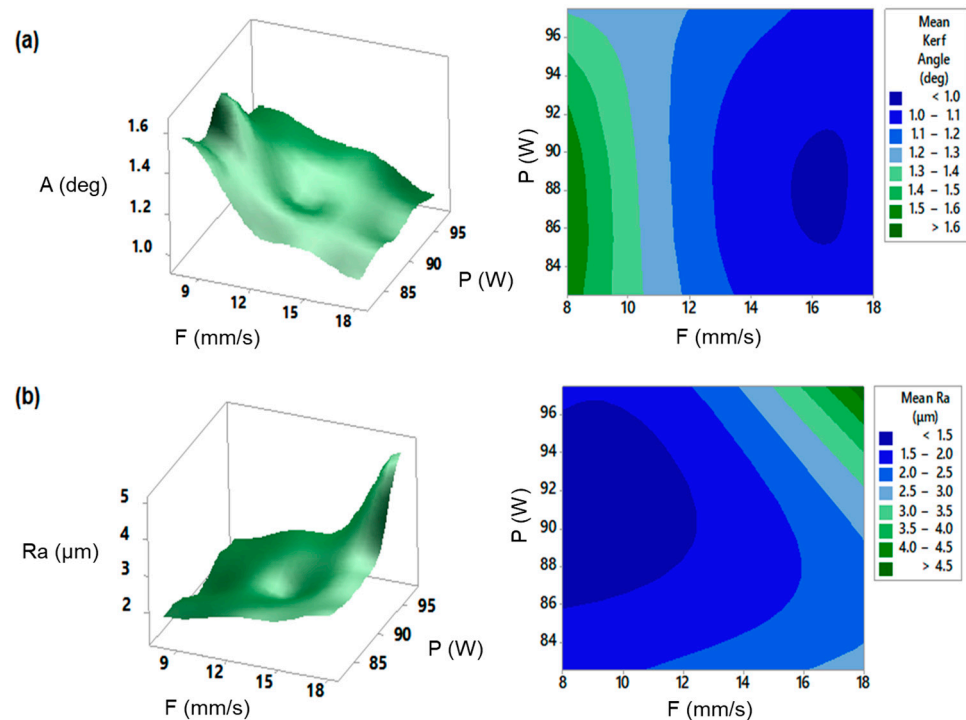


Figure 4. Surface and contour plots for the objectives of: (a) mean kerf angle, (b) mean surface roughness.

Surface and contour plots represent the simultaneous effect of laser feed and laser power on mean kerf angle (Figure 4a) and mean surface roughness (Figure 4b). It can be observed that when increased, laser feed ( $F$ ) tends to reduce kerf angle, provided that laser power is set to high levels, i.e., 97.5 (W). In the case of mean surface roughness,  $R_a$  lower levels for laser feed need to be set. Laser power must be set with a value between 86 (W) and 96–97 (W), approximately. The trend in the response surfaces and contour plots shows that the LC problem is highly nonlinear, even when studying two independent process parameters on discrete objectives such as those selected in this work: mean  $A$  and  $R_a$ . The regression equations corresponding to these plots for mean  $A$  and  $R_a$ , with reference to the general equation shown in Equation (1), are given in Equations (2) and (3).

$$A (^{\circ}) = 0.98 - 0.3177 \times F + 0.0615 \times P + 0.00464 \times F^2 - 0.000493 \times P^2 + 0.001682 \times F \times P, \tag{2}$$

$$Ra (\mu\text{m}) = 123.8 - 1.734 \times F - 2.536 \times P + 0.01947 \times F^2 + 0.01320 \times P^2 + 0.01566 \times F \times P \tag{3}$$

The ANOVA corresponding to the regression models for mean kerf angle and mean Ra is summarized in Table 3.

**Table 3.** ANOVA results for A and Ra regression models.

Source	DF	Seq.SS	% Contribution	Adj.SS	Adj.MS	F-Value	P-Value
F(mm/s)	1	0.93298	76.86	0.93298	0.932978	165.59	0.000
P(W)	1	0.02936	2.42	0.02936	0.029363	5.21	0.033
F <sup>2</sup>	1	0.08089	6.66	0.08089	0.080891	14.36	0.001
P <sup>2</sup>	1	0.00461	0.38	0.00461	0.004611	0.82	0.376
F × P	1	0.04775	3.93	0.04775	0.047754	8.48	0.008
Error	21	0.11832	9.75	0.11832	0.005634		
Total	26	1.21392	100.00				
A model R <sup>2</sup>		90.25%					
F(mm/s)	1	14.706	51.69	14.706	14.7063	103.73	0.000
P(W)	1	1.905	6.69	1.905	1.9045	13.43	0.001
F <sup>2</sup>	1	1.421	4.99	1.421	1.4211	10.02	0.005
P <sup>2</sup>	1	3.308	11.63	3.308	3.3078	23.33	0.000
F × P	1	4.136	14.54	4.136	4.1360	29.17	0.000
Error	21	2.977	10.46	2.977	0.1418		
Total	26	28.453	100.00				
Ra model R <sup>2</sup>		89.54%					

The probability of an F-value greater than the calculated F-value due to noise is indicated by the P-value. Therefore, if the P-value is less than 0.05, the importance of the related term is specified. Otherwise, if the P-value is higher than 0.05, a lack of fit exists. A negligible lack of fit is desirable because it indicates that any term excluded by the model is minor and that the developed model serves well. Finally, the normality test (Anderson–Darling) is employed to confirm the suitability of the models corresponding to the mean A and Ra. If the P-value for the normality test is lower than 0.05, it is supposed that the data do not follow a normal distribution. In this work, ANOVA indicates that both quadratic models are suitable for predicting the mean A and mean Ra with high contributions, i.e., 90.25% and 89.54%.

### 3.2. Validation

The adequacy of regression models for predicting the objectives of interest is validated by the Anderson–Darling normality test, where the P-value for normality plots is examined and should be found well above 0.05 in order to indicate that residuals follow a normal distribution. Suppose the P-values for residuals are located well above 0.05. In that case, the regression equations can be considered adequate to use the models to predict the responses and claim that they agree with experimental results. Figure 5 illustrates the results obtained by the Anderson–Darling normality test applied to the residuals obtained by ANOVA analysis for both regression models. Figure 5a presents the results corresponding to the mean kerf angle, while Figure 5b corresponds to the results concerning mean surface roughness. P-values corresponding to the residuals of mean kerf angle and mean surface roughness are equal to 0.478 and 0.390, respectively, and are well above 0.05. Therefore, the models agree with experimental results and can be used for predicting the responses.

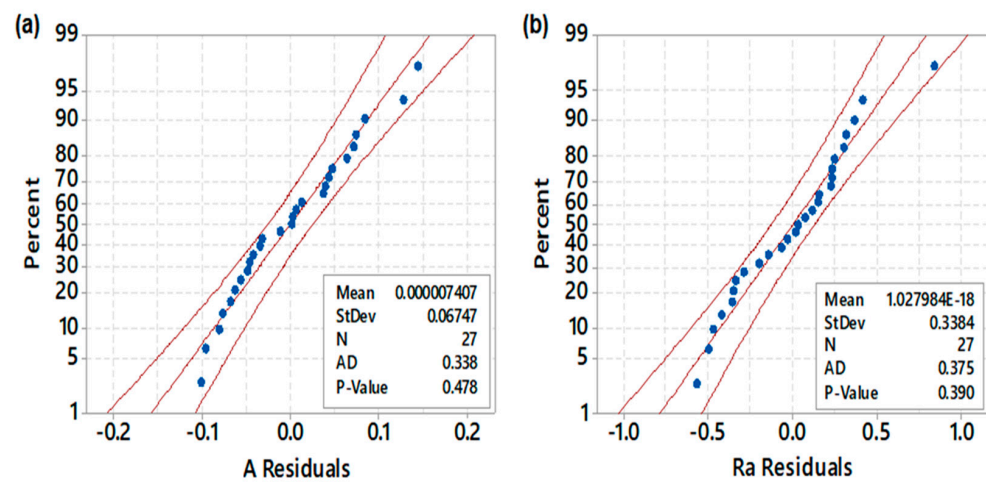


**Figure 5.** Normal probability plots of residuals for: (a) mean kerf angle, (b) mean surface roughness.

### 3.3. Neural Network Prediction

It has been shown that laser cutting operation exhibits high complexity despite the fact that only two independent variables have been considered (laser feed and laser power). This complexity may introduce difficulties in accurate response predictions using conventional approaches. To further examine the potential of accurate response prediction, several neural network architectures have been examined to obtain a reliable neural network capable of predicting both responses. In the current work, laser feed and laser power were considered as the two input parameters. Each of the parameters are represented by a single neuron and, consequently, the input layer in the neural network structure comprises two neurons. To introduce a reliable database to the network, the experimental results were considered, referring to the outputs and the independent variables along with their limit ranges. Results for kerf angle and surface roughness were used for training the network and examine the input–output correlation. Thereby, the database was divided into three discrete datasets, namely the training, testing, and validation (random selection of data division; 70% for training, 15% for validating, and 15% for testing). The training set was thoroughly used for adjusting the weights, the testing set was used for examining the network’s accuracy in its predictions, and the validation set was used for validating the results according to the training procedure. Consequently, the experiments were divided into three sets: thirty-eight for training, eight for validation, and eight for testing, i.e., fifty-six experimental data. Note here that Table 2 contains twenty-seven measurements for mean Ra and mean A, which were produced each by twenty-seven average values in the X and twenty-seven in the Y direction, and therefore fifty-six values were used for NN modelling.

Neural network training deals with the update in its connected weights so that the error among predicted and actual experimental outputs is minimized. The neural network architectures examined were tested using the standard backpropagation algorithm found in Mathworks® MATLAB® R2014b. In order to decide the final number of neurons referring to the hidden layer, several structures under a varying number of neurons were tested according to the methodology explained in [43]. The activation level for the neurons was determined by the tan-sigmoid transfer function, while “trainlm” was the training function. It was found that the 2-8-2 network topology was the most beneficial among those examined. Additionally, 0.001 mu (learning rate), 0.1 mu+ (increment factor), and 10 mu– (decrement factor) were decided upon.

This topology ended up with the best result for validation performance, equal to 0.029731 at epoch 5 and after 100 iterative evaluations. Figure 6a illustrates the ANN architecture with k = 8 neurons for the hidden layer, and Figure 6b shows the train, test, and validation results corresponding to the best validation performance (0.029731) and epochs.

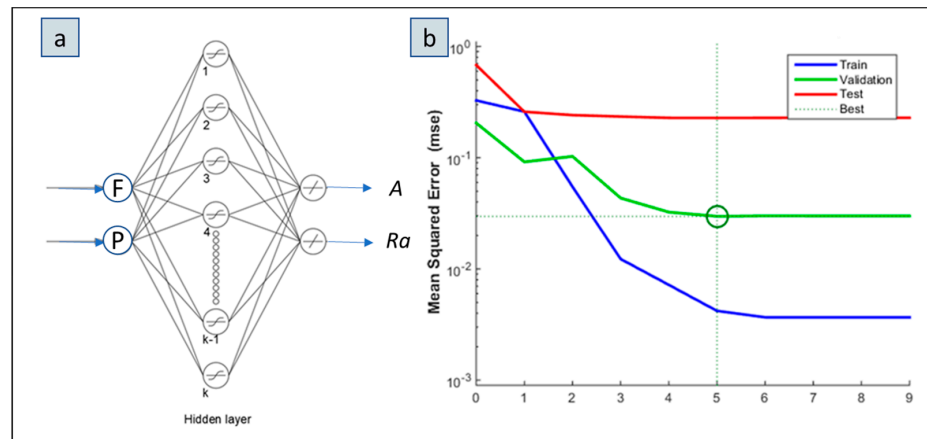


Figure 6. (a) Graphical illustration of the ANN architecture; (b) ANN validation performance.

To verify the prominence of this trained ANN architecture, the training set was presented to the ANN. Figure 7 depicts the regression analysis among the ANN response and related targets. It can be observed that there was a high correlation coefficient (R) among the outputs (predicted results), and the targets verify the ANN’s performance.

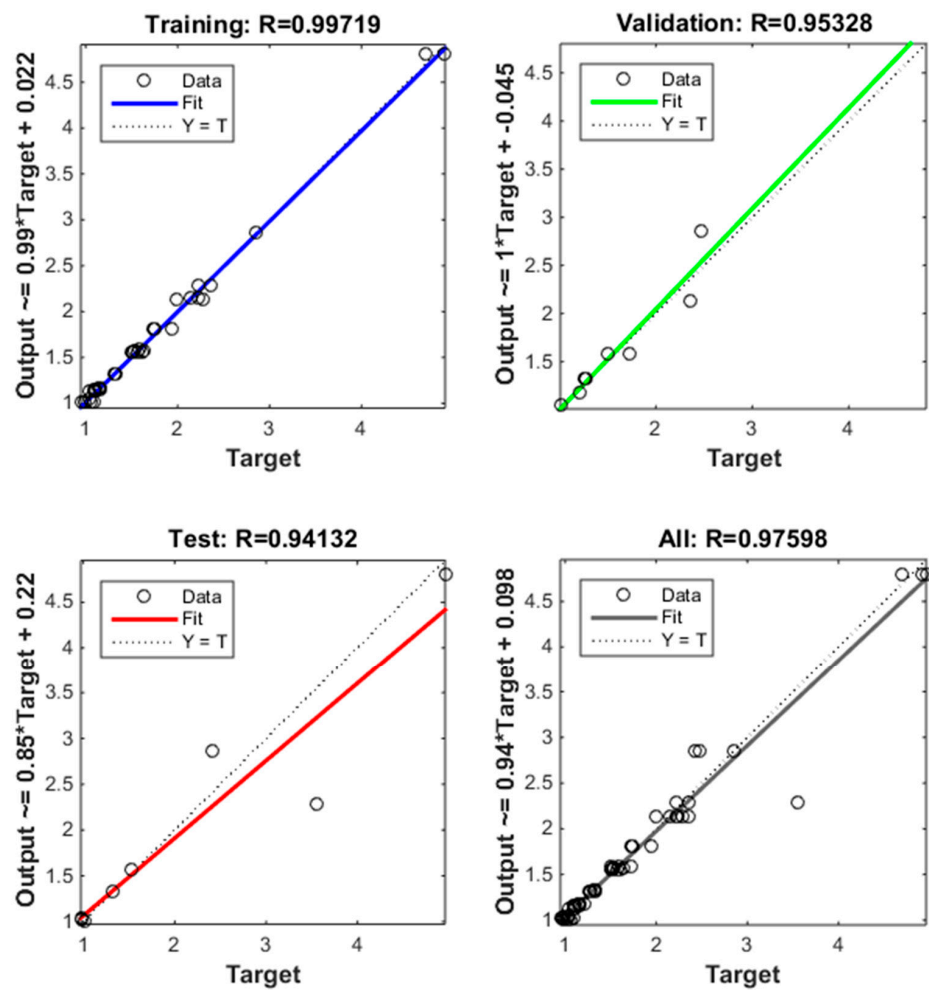


Figure 7. Regression analysis results obtained by the ANN architecture adopted, based on its validation performance.

A comparison of the experimental results, the results predicted by the regression models, and the results predicted by the ANN are shown in Figure 8. Figure 8a refers to the results concerning the mean kerf angle, while Figure 8b refers to the results for mean surface roughness. It can be observed that both regression and ANN analysis exhibit almost equal prediction potentials referring to the objectives of mean kerf angle and surface roughness and the system’s nonlinear behavior.

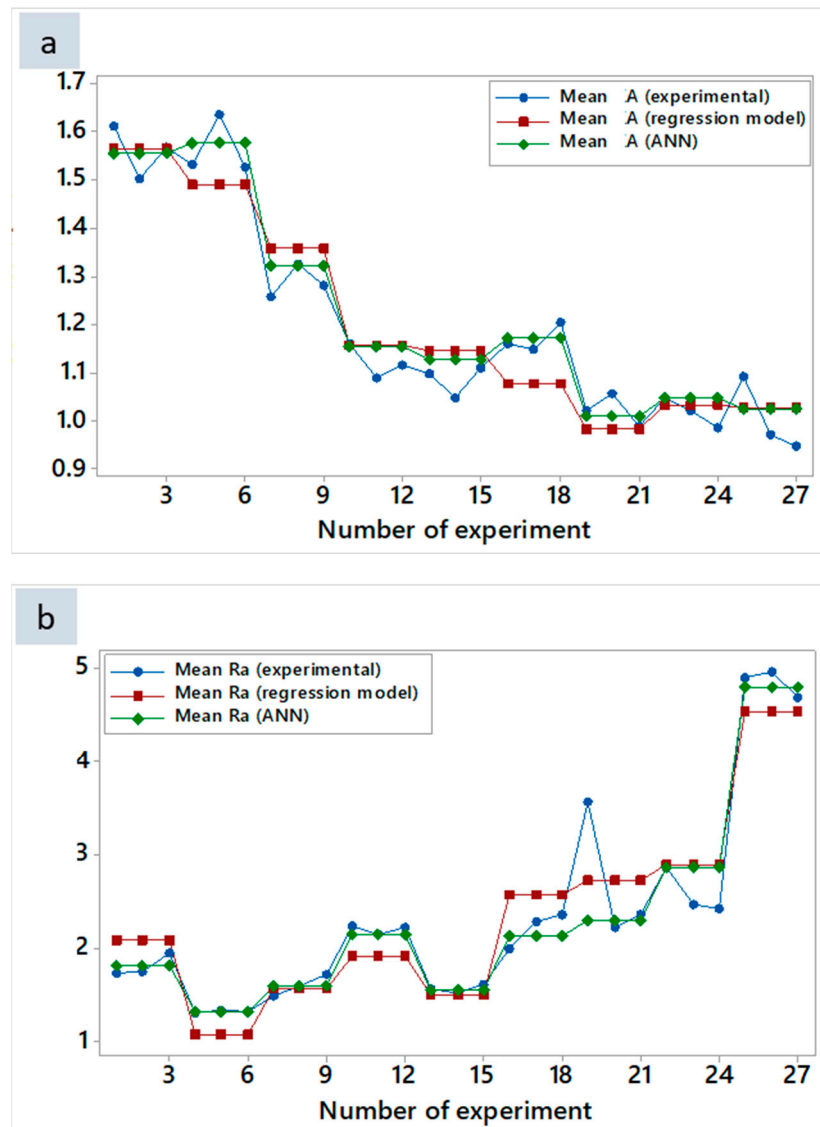


Figure 8. Comparison among experimental results, regression model, and ANN for (a) mean kerf angle and (b) mean surface roughness.

### 3.4. Multi-Objective Optimization of CO<sub>2</sub> LC Parameters

The optimization problem formulated in this work was based on the regression equations presented in Equations (2) and (3) for predicting mean kerf angle and mean surface roughness. The objective function, control parameters, and their optimization bounds considered are the same as those presented in the experimental design. In this two-objective optimization case, the two control parameters of laser feed and laser power were examined in a continuous form. The problem was solved by employing the multi-objective grey wolf optimization algorithm (MOGWO) developed by Mirjalili et al. [44]. The optimization problem was solved using a population size of grey wolves equal to 20 and a maximum number of generations equal to 1000 (i.e., a maximum number of

function evaluations equal to 20,000). Since the current work is purely experimental, no comparative results based on multiple algorithmic simulations were produced using other competitive metaheuristics. Therefore, no statistical outputs are presented in this work. It is in the scope of the authors’ future research to compare several algorithms in terms of their performance on this problem and other manufacturing-related multi-objective problems for optimization.

The results obtained by the MOGWO algorithm are presented in the form of non-dominated optimal solutions in a Pareto front. The trend in the Pareto front representing the non-dominated optimal solutions clearly reveals the trade-off between the two objectives of minimum kerf angle and minimum surface roughness, mainly owing to laser feed. By examining the experimental results presented in the form of contour and surface plots, it can be deduced that optimization outputs are well-supported. The non-dominated optimal solutions are depicted in Figure 9, and they are also tabulated in Table 4.

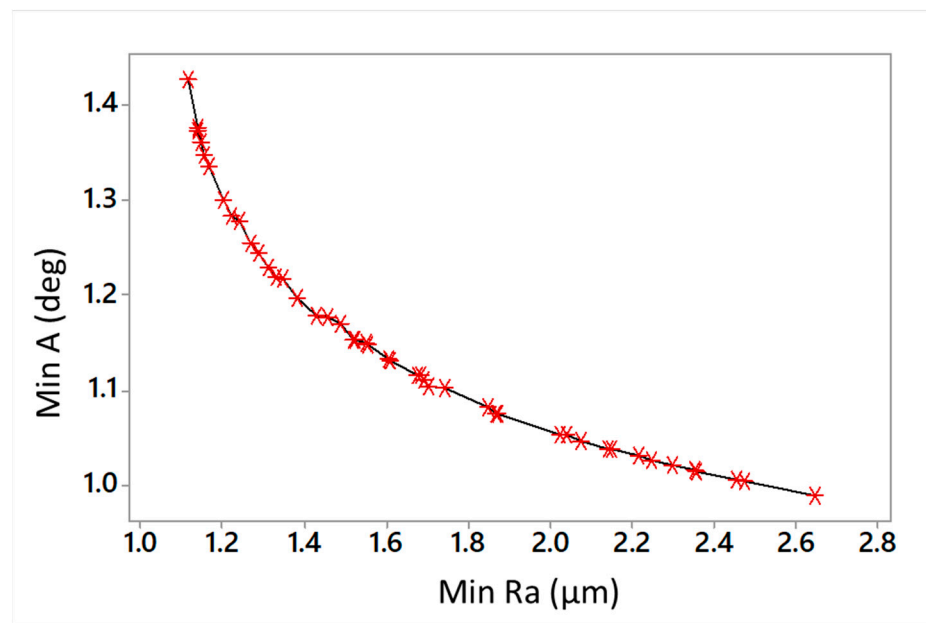


**Figure 9.** Non-dominated, “Pareto optimal” solutions, obtained by MOGWO algorithm for solving the CO<sub>2</sub> laser cutting problem.

**Table 4.** Recommended optimal solutions for minKA and minRa by MOGWO algorithm.

Sol. No.	Optimization Objectives		Control Parameters	
	minA (°)	minRa (µm)	F (mm/s)	P (W)
1	0.98822	2.64480	17.48111	82.50000
2	1.07466	1.87228	14.92668	86.77339
3	1.42772	1.11480	08.53595	90.92663
4	1.27861	1.23830	10.71434	89.29454
5	1.33577	1.16668	09.66419	91.03837
6	1.02117	2.29789	16.40072	83.83890
7	1.07543	1.86701	14.91328	87.15281
8	1.03065	2.21364	16.11121	84.18711
9	1.29996	1.20229	10.20007	90.76634
10	1.00332	2.47574	16.99961	83.21187
11	1.10474	1.70393	14.09902	87.58292
12	1.00525	2.45430	16.91170	83.22919
13	1.19700	1.38032	12.04552	89.16643
14	1.11602	1.67524	13.84686	86.67821
15	1.15247	1.52201	13.01707	87.74314

Table 4. Cont.

Sol. No.	Optimization Objectives		Control Parameters	
	minA (°)	minRa (µm)	F (mm/s)	P (W)
16	1.01505	2.35604	16.64665	83.78354
17	1.03745	2.15047	16.00275	84.95377
18	1.11079	1.68988	13.96640	86.86978
19	1.05329	2.02306	15.53363	85.66028
20	1.37699	1.13618	09.18147	90.72416
21	1.36152	1.14691	09.41792	90.46029
22	1.37215	1.13903	09.24583	90.70076
23	1.08154	1.84548	14.70373	86.03587
24	1.21654	1.34745	11.76379	88.63053
25	1.14929	1.54881	13.11347	87.17124
26	1.13218	1.60573	13.47646	87.05567
27	1.13155	1.60924	13.49164	87.01271
28	1.28392	1.22144	10.53108	90.08822
29	1.21911	1.33139	11.64764	89.29424
30	1.22900	1.31082	11.46317	89.46176
31	1.14719	1.55199	13.15207	87.25544
32	1.11552	1.68425	13.86107	86.47686
33	1.10185	1.73947	14.18546	86.43617
34	1.17593	1.45489	12.55105	87.87838
35	1.17909	1.42963	12.42239	88.69144
36	1.34805	1.15551	09.57331	90.58348
37	1.24481	1.28694	11.24017	89.20021
38	1.03864	2.14012	15.97860	85.07588
39	1.24427	1.28737	11.24562	89.22634
40	1.15305	1.51632	12.99429	87.91324
41	1.01524	2.35420	16.64214	83.79649
42	1.25371	1.26658	11.03781	89.70594
43	1.05238	2.03865	15.49707	85.07198
44	1.24447	1.28734	11.24459	89.20843
45	1.24447	1.28734	11.24459	89.20843
46	1.04677	2.07469	15.71065	85.26258
47	1.02666	2.24627	16.28398	84.26596
48	1.24447	1.28734	11.24459	89.20843
49	1.16961	1.48469	12.70009	87.44660
50	1.24447	1.28734	11.24459	89.20843

By looking at the Pareto front, the spread of non-dominated solutions is uniformly distributed along the path line, while they almost equidistantly cover its trend, suggesting both coverage and spacing. This is very important when it comes to the selection of several solutions depending upon different requirements referring to the objectives. It is evident that no combinatorial solution such as the non-dominated solutions in multi-objective problems can simultaneously satisfy the objectives involved in the same degree. One objective will always be optimized at the expense of the rest. However, it is important to maintain advantageous outputs regardless of the trade-off among the antagonizing solutions. A typical example is shown through the combination between the results obtained by the MOGWO algorithm for the minimum mean kerf angle and minimum mean surface roughness in the first solution (Table 4). Based on the experimental results, the minimum attainable value for the mean kerf angle is found to equal  $0.884^\circ$ , corresponding to the value of  $5.92 \mu\text{m}$  for mean surface roughness. The minimum value for mean kerf angle obtained by the MOGWO algorithm was found to equal  $0.988^\circ$ . This result is 10.53% worse compared to the actual experimental value of  $0.884^\circ$  for mean kerf angle. However, this result corresponds to the value of  $2.645 \mu\text{m}$  for minimum mean surface roughness (see solution number 1 in Table 4). This result is 55.32% more beneficial at the expense of mean kerf angle. It should also be noted that the gain among the different non-dominated

optimal solutions depends on the quality of predictions by regression models rather than the algorithm itself. If the experimental error is low, then there is a higher chance that regression modeling will attain a higher correlation among control factors and responses. Thereby, the resulting non-dominated solutions will occur with higher quality and overall gain. The maximum (worst) experimental result for mean kerf angle is  $1.612^\circ$  against the maximum (worst) result obtained by MOGWO, which is  $1.4277^\circ$ . In other words, the worst result corresponding to the non-dominated solution for mean kerf angle is 11.43% more beneficial than that which appeared in the actual experiment. Similarly, the maximum (worst) experimental result for mean surface roughness is  $6.19 \mu\text{m}$  against the maximum (worst) result obtained by MOGWO, which is  $2.6448 \mu\text{m}$ . This means that the worst result corresponding to the non-dominated solution for mean surface roughness is 57.27% more beneficial compared to the actual experimental result. The computational time required by the MOGWO algorithm to perform 20,000 function evaluations was approximately 2 min.

#### 4. Conclusions

This work examines the results of two key parameters, laser feed and laser power, on the responses of mean Ra and mean A when it comes to the CO<sub>2</sub> laser cutting of 3DP polylactic acid (PLA) plates. The responses were modeled using regression analysis and neural networks whilst being simultaneously optimized by implementing the grey wolf optimization algorithm (MOGWO) adopted from the literature. The findings of this work are summarized below:

- The kerf angle and Ra of the PLA 3DP samples cut by the CO<sub>2</sub> laser are affected by the direction of the filament strands during the 3DP, as well as feed (F) and power (P) parameters.
- In general, when laser feed increases or the power decreases, the energy per unit area decreases, resulting in smaller bottom kerf widths and energy redistribution inside the cutting area.
- ANOVA and statistics show that feed is the dominant parameter for both responses, having the power to be rather significant for mean Ra. By examining the contour plots and response surfaces, we concluded that the interaction between laser feed and power is synergistic for mean A and antagonistic for mean Ra.
- The feed parameter exhibits approximately 77% contribution in terms of its effect on the mean kerf angle. This contribution is followed by the effect of the square term of feed (6.66%), the interaction effect between feed and power (3.93%), and the effect of power (2.42%). Therefore, the correlation coefficient for the regression model to predict mean A was equal to 90.25%.
- The feed parameter also exhibits a high contribution percentage for the response of mean Ra (51.69%). The second contribution effect is seen through the interaction between feed and power (14.54%), followed by the square term of power (11.63%). The rest of the parameter effects are less significant for mean Ra. The correlation coefficient for the regression model to predict mean A is equal to 89.54%.
- The topology of 2-8-2 for the layers of a backpropagation ANN seems to be quite promising in predicting the responses of mean A and Ra, with high correlation.
- The non-dominated set of Pareto optimal solutions seems advantageous for different importance degrees among mean kerf angle and surface roughness. Their inherent trade-off results from the nonlinear behavior, mainly owing to feed. A general range in terms of the overall gain by employing some indicative optimal solutions is between 10 and 55%.

In this manuscript, we formulated a two-objective optimization problem based on the two objectives of mean kerf angle and surface roughness. According to the “non-dominated” set of solutions theory, it would be difficult to emphasize the best parameter settings for the objectives. In a multi-objective optimization problem (i.e., two objectives), the end user should decide which non-dominated solution is to be selected according to the process requirements, constraints, and technical specifications. The Pareto front

should be carefully examined, and a “bi-objective” solution should be selected, with the recommended settings for its process parameters referring to both laser power and laser feed. To assist with process planning for laser cutting and to recommend a range of “best” solutions, one should restrict their selections to the Pareto points existing on the curved space of the front. These solutions are closer to the axes’ origin, thus simultaneously minimizing both objectives to the best possible extent.

Looking further ahead, the authors plan to study other LC operations for several 3DP materials, examine the effect among crucial laser and 3D printing parameters, and optimize more responses related to quality and productivity (heat affected zone, dross, energy consumption, etc.) by implementing different modern metaheuristics and intelligent algorithms. Additionally, note that the infill structure of 3D-printed parts can vary even for the same material and geometry by changing the infill parameters or fabrication orientation, affecting laser cutting performance.

**Author Contributions:** Conceptualization, J.D.K.; methodology, N.A.F.; software, N.A.F.; validation, K.N.; formal analysis, K.N.; investigation, N.A.F. and K.N.; resources, J.D.K.; data curation, K.N.; writing—original draft preparation, J.D.K., N.A.F. and N.M.V.; writing—review and editing, J.D.K. and N.M.V.; visualization, J.D.K.; supervision, J.D.K. and N.M.V.; project administration, J.D.K.; funding acquisition, J.D.K. All authors have read and agreed to the published version of the manuscript.

**Funding:** This research received no external funding.

**Data Availability Statement:** All data required to reproduce these findings are included in this manuscript.

**Conflicts of Interest:** The authors declare no conflict of interest.

## References

1. Stavropoulos, P.; Koutsomichalis, A.; Vaxevanidis, N. Laser-Based Manufacturing Processes for Aerospace Applications. In *Materials Science and Engineering*; IGI Global: Hershey, PA, USA, 2017; pp. 374–391. [\[CrossRef\]](#)
2. Mushtaq, R.T.; Wang, Y.; Rehman, M.; Khan, A.M.; Mia, M. State-of-the-Art and Trends in CO<sub>2</sub> Laser Cutting of Polymeric Materials—A Review. *Materials* **2020**, *13*, 3839. [\[CrossRef\]](#) [\[PubMed\]](#)
3. Ninikas, K.; Kechagias, J.; Salonitis, K. The Impact of Process Parameters on Surface Roughness and Dimensional Accuracy during CO<sub>2</sub> Laser Cutting of PMMA Thin Sheets. *J. Manuf. Mater. Process.* **2021**, *5*, 74. [\[CrossRef\]](#)
4. Förster, D.J.; Jäggi, B.; Michalowski, A.; Neuenschwander, B. Review on Experimental and Theoretical Investigations of Ultra-Short Pulsed Laser Ablation of Metals with Burst Pulses. *Materials* **2021**, *14*, 3331. [\[CrossRef\]](#) [\[PubMed\]](#)
5. Sing, S.L.; Kuo, C.N.; Shih, C.T.; Ho, C.C.; Chua, C.K. Perspectives of Using Machine Learning in Laser Powder Bed Fusion for Metal Additive Manufacturing. *Virtual Phys. Prototyp.* **2021**, *16*, 372–386. [\[CrossRef\]](#)
6. Al-Ahmari, A.M.A.; Rasheed, M.S.; Mohammed, M.K.; Saleh, T. A Hybrid Machining Process Combining Micro-EDM and Laser Beam Machining of Nickel–Titanium-Based Shape Memory Alloy. *Mater. Manuf. Process.* **2016**, *31*, 447–455. [\[CrossRef\]](#)
7. Buj-Corral, I.; Bagheri, A.; Sivatte-Adroer, M. Effect of Printing Parameters on Dimensional Error, Surface Roughness and Porosity of FFF Printed Parts with Grid Structure. *Polymers* **2021**, *13*, 1213. [\[CrossRef\]](#)
8. Elkaseer, A.; Schneider, S.; Scholz, S.G. Experiment-Based Process Modeling and Optimization for High-Quality and Resource-Efficient FFF 3D Printing. *Appl. Sci.* **2020**, *10*, 2899. [\[CrossRef\]](#)
9. Fountas, N.A.; Kechagias, J.D.; Manolakos, D.E.; Vaxevanidis, N.M. Single and Multi-Objective Optimization of FDM-Based Additive Manufacturing Using Metaheuristic Algorithms. *Procedia Manuf.* **2020**, *51*, 740–747. [\[CrossRef\]](#)
10. Kim, H.; Lin, Y.; Tseng, T.-L.B. A Review on Quality Control in Additive Manufacturing. *Rapid Prototyp. J.* **2018**, *24*, 645–669. [\[CrossRef\]](#)
11. Milovanovic, S.; Pajnik, J.; Lukic, I. Tailoring of Advanced Poly (Lactic Acid)-based Materials: A Review. *J. Appl. Polym. Sci.* **2022**, *139*, 51839. [\[CrossRef\]](#)
12. Gul, J.Z.; Sajid, M.; Rehman, M.M.; Siddiqui, G.U.; Shah, I.; Kim, K.-H.; Lee, J.-W.; Choi, K.H. 3D Printing for Soft Robotics—A Review. *Sci. Technol. Adv. Mater.* **2018**, *19*, 243–262. [\[CrossRef\]](#) [\[PubMed\]](#)
13. Buj-Corral, I.; Sánchez-Casas, X.; Luis-Pérez, C.J. Analysis of AM Parameters on Surface Roughness Obtained in PLA Parts Printed with FFF Technology. *Polymers* **2021**, *13*, 2384. [\[CrossRef\]](#) [\[PubMed\]](#)
14. Wong, K.V.; Hernandez, A. A Review of Additive Manufacturing. *ISRN Mech. Eng.* **2012**, *2012*, 208760. [\[CrossRef\]](#)
15. Pham, D.T.; Gault, R.S. A comparison of rapid prototyping technologies. *Int. J. Mach. Tools Manuf.* **1998**, *38*, 1257. [\[CrossRef\]](#)
16. Kechagias, J.D.; Zaoutsos, S.P. Optimising Fused Filament Fabrication Surface Roughness for a Dental Implant. *Mater. Manuf. Process.* **2023**, *38*, 954–959. [\[CrossRef\]](#)

17. Kechagias, J.; Chaidas, D. Fused Filament Fabrication Parameter Adjustments for Sustainable 3D Printing. *Mater. Manuf. Process.* **2023**, *38*, 933–940. [[CrossRef](#)]
18. Faludi, J.; Bayley, C.; Bhogal, S.; Iribarne, M. Comparing Environmental Impacts of Additive Manufacturing vs. Traditional Machining via Life-Cycle Assessment. *Rapid Prototyp. J.* **2015**, *21*, 14–33. [[CrossRef](#)]
19. Correa-Pacheco, Z.N.; Black-Solis, J.D.; Ortega-Gudiño, P.; Sabino-Gutiérrez, M.A.; Benítez-Jiménez, J.J.; Barajas-Cervantes, A.; Bautista-Baños, S.; Hurtado-Colmenares, L.B. Preparation and Characterization of Bio-Based PLA/PBAT and Cinnamon Essential Oil Polymer Fibers and Life-Cycle Assessment from Hydrolytic Degradation. *Polymers* **2019**, *12*, 38. [[CrossRef](#)]
20. Nofar, M.; Salehiyan, R.; Sinha Ray, S. Rheology of Poly (Lactic Acid)-Based Systems. *Polym. Rev.* **2019**, *59*, 465–509. [[CrossRef](#)]
21. Fortelny, I.; Ujčić, A.; Fambri, L.; Slouf, M. Phase Structure, Compatibility, and Toughness of PLA/PCL Blends: A Review. *Front. Mater.* **2019**, *6*, 206. [[CrossRef](#)]
22. Davim, J.P.; Barricas, N.; Conceição, M.; Oliveira, C. Some Experimental Studies on CO<sub>2</sub> Laser Cutting Quality of Polymeric Materials. *J. Mater. Process. Technol.* **2008**, *198*, 99–104. [[CrossRef](#)]
23. Caiazzo, F.; Curcio, F.; Daurelio, G.; Minutolo, F.M.C. Laser Cutting of Different Polymeric Plastics (PE, PP and PC) by a CO<sub>2</sub> Laser Beam. *J. Mater. Process. Technol.* **2005**, *159*, 279–285. [[CrossRef](#)]
24. Choudhury, I.A.; Shirley, S. Laser Cutting of Polymeric Materials: An Experimental Investigation. *Opt. Laser Technol.* **2010**, *42*, 503–508. [[CrossRef](#)]
25. Kechagias, J.; Ninikas, K.; Stavropoulos, P.; Salonitis, K. A Generalised Approach on Kerf Geometry Prediction during CO<sub>2</sub> Laser Cut of PMMA Thin Plates Using Neural Networks. *Lasers Manuf. Mater. Process.* **2021**, *8*, 372–393. [[CrossRef](#)]
26. Stankova, N.; Nikolov, A.; Iordanova, E.; Yankov, G.; Nedyalkov, N.; Atanasov, P.; Tatchev, D.; Valova, E.; Kolev, K.; Armyanov, S.; et al. New Approach toward Laser-Assisted Modification of Biocompatible Polymers Relevant to Neural Interfacing Technologies. *Polymers* **2021**, *13*, 3004. [[CrossRef](#)]
27. Zhou, B.H.; Mahdavian, S.M. Experimental and Theoretical Analyses of Cutting Nonmetallic Materials by Low Power CO<sub>2</sub>-Laser. *J. Mater. Process. Technol.* **2004**, *146*, 188–192. [[CrossRef](#)]
28. Moradi, M.; Karami Moghadam, M.; Shamsborhan, M.; Bodaghi, M.; Falavandi, H. Post-Processing of FDM 3D-Printed Polylactic Acid Parts by Laser Beam Cutting. *Polymers* **2020**, *12*, 550. [[CrossRef](#)]
29. Kechagias, J.D.; Fountas, N.A.; Ninikas, K.; Petousis, M.; Vidakis, N.; Vaxevanidis, N. Surface Characteristics Investigation of 3D-Printed PET-G Plates during CO<sub>2</sub> Laser Cutting. *Mater. Manuf. Process.* **2021**, *37*, 1446–1462. [[CrossRef](#)]
30. Kechagias, J.; Ninikas, K.; Petousis, M.; Vidakis, N. Laser Cutting of 3D Printed Acrylonitrile Butadiene Styrene Plates for Dimensional and Surface Roughness Optimization. *Int. J. Adv. Manuf. Technol.* **2022**, *119*, 2301–2315. [[CrossRef](#)]
31. Kechagias, J.; Ninikas, K.; Petousis, M.; Vidakis, N.; Vaxevanidis, N. An Investigation of Surface Quality Characteristics of 3D Printed PLA Plates Cut by CO<sub>2</sub> Laser Using Experimental Design. *Mater. Manuf. Process.* **2021**, *36*, 1544–1553. [[CrossRef](#)]
32. Yang, L.; Wei, J.; Ma, Z.; Song, P.; Ma, J.; Zhao, Y.; Huang, Z.; Zhang, M.; Yang, F.; Wang, X. The Fabrication of Micro/Nano Structures by Laser Machining. *Nanomaterials* **2019**, *9*, 1789. [[CrossRef](#)]
33. Kechagias, J.D.; Vidakis, N.; Ninikas, K.; Petousis, M.; Vaxevanidis, N.M. Hybrid 3D Printing of Multifunctional Polylactic Acid/Carbon Black Nanocomposites Made with Material Extrusion and Post-Processed with CO<sub>2</sub> Laser Cutting. *J. Adv. Manuf. Technol.* **2023**, *124*, 1843–1861. [[CrossRef](#)]
34. Shakeri, Z.; Benfriha, K.; Shirinbayan, M.; Ahmadifar, M.; Tcharkhtchi, A. Mathematical Modeling and Optimization of Fused Filament Fabrication (FFF) Process Parameters for Shape Deviation Control of Polyamide 6 Using Taguchi Method. *Polymers* **2021**, *13*, 3697. [[CrossRef](#)] [[PubMed](#)]
35. Bedi, R.; Mehta, B. Adaptive Neuro Fuzzy Inference System in Modelling/Detecting Cracks and Porosity Using Liquid Penetrant Test. *Int. J. Exp. Des. Process Optim.* **2016**, *5*, 117. [[CrossRef](#)]
36. Jones, B.; Montgomery, D.C. Alternatives to Resolution IV Screening Designs in 16 Runs. *Int. J. Exp. Des. Process Optim.* **2010**, *1*, 285. [[CrossRef](#)]
37. Kechagias, J.D.; Aslani, K.-E.; Fountas, N.A.; Vaxevanidis, N.M.; Manolakos, D.E. A Comparative Investigation of Taguchi and Full Factorial Design for Machinability Prediction in Turning of a Titanium Alloy. *Measurement* **2020**, *151*, 107213. [[CrossRef](#)]
38. Madić, M.; Petrović, G.; Petković, D.; Antucheviciene, J.; Marinković, D. Application of a Robust Decision-Making Rule for Comprehensive Assessment of Laser Cutting Conditions and Performance. *Machines* **2022**, *10*, 153. [[CrossRef](#)]
39. Haddadi, E.; Moradi, M.; Karimzad Ghavidel, A.; Karimzad Ghavidel, A.; Meibadi, S. Experimental and Parametric Evaluation of Cut Quality Characteristics in CO<sub>2</sub> Laser Cutting of Polystyrene. *Optik* **2019**, *184*, 103–114. [[CrossRef](#)]
40. Tamrin, K.F.; Nukman, Y.; Sheikh, N.A. Laser Spot Welding of Thermoplastic and Ceramic: An Experimental Investigation. *Mater. Manuf. Process.* **2015**, *30*, 1138–1145. [[CrossRef](#)]
41. Kurt, M.; Kaynak, Y.; Bagci, E.; Demirer, H.; Kurt, M. Dimensional Analyses and Surface Quality of the Laser Cutting Process for Engineering Plastics. *Int. J. Adv. Manuf. Technol.* **2009**, *41*, 259–267. [[CrossRef](#)]
42. Andriushchenko, E.; Kallaste, A.; Belahcen, A.; Vaimann, T.; Rassõlkin, A.; Heidari, H.; Tiismus, H. Optimization of a 3D-Printed Permanent Magnet Coupling Using Genetic Algorithm and Taguchi Method. *Electronics* **2021**, *10*, 494. [[CrossRef](#)]

43. Kechagias, J.D.; Tsiolikas, A.; Petousis, M.; Ninikas, K.; Vidakis, N.; Tzounis, L. A robust methodology for optimizing the topology and the learning parameters of an ANN for accurate predictions of laser-cut edges surface roughness. *Simul. Model. Pract. Theory* **2022**, *114*, 102414. [[CrossRef](#)]
44. Mirjalili, S.; Saremi, S.; Mirjalili, S.M.; Coelho, L.D.S. Multi-Objective Grey Wolf Optimizer: A Novel Algorithm for Multi-Criterion Optimization. *Expert Syst. Appl.* **2016**, *47*, 106–119. [[CrossRef](#)]

**Disclaimer/Publisher's Note:** The statements, opinions and data contained in all publications are solely those of the individual author(s) and contributor(s) and not of MDPI and/or the editor(s). MDPI and/or the editor(s) disclaim responsibility for any injury to people or property resulting from any ideas, methods, instructions or products referred to in the content.